
Training-free Diffusion Model Adaptation for Variable-Sized Text-to-Image Synthesis

Zhiyu Jin¹, Xuli Shen^{1,2}, Bin Li^{1*}, Xiangyang Xue¹

¹ Shanghai Key Laboratory of Intelligent Information Processing
School of Computer Science, Fudan University

² UniDT Technology

Abstract

Diffusion models (DMs) have recently gained attention with state-of-the-art performance in text-to-image synthesis. Abiding by the tradition in deep learning, DMs are trained and evaluated on the images with fixed sizes. However, users are demanding for various images with specific sizes and various aspect ratio. This paper focuses on adapting text-to-image diffusion models to handle such variety while maintaining visual fidelity. First we observe that, during the synthesis, lower resolution images suffer from incomplete object portrayal, while higher resolution images exhibit repetitively disordered presentation. Next, we establish a statistical relationship indicating that attention entropy changes with token quantity, suggesting that models aggregate spatial information in proportion to image resolution. The subsequent interpretation on our observations is that objects are incompletely depicted due to limited spatial information for low resolutions, while repetitively disorganized presentation arises from redundant spatial information for high resolutions. From this perspective, we propose a scaling factor to alleviate the change of attention entropy and mitigate the defective pattern observed. Extensive experimental results validate the efficacy of the proposed scaling factor, enabling models to achieve better visual effects, image quality, and text alignment. Notably, these improvements are achieved without additional training or fine-tuning techniques.

1 Introduction

Diffusion models have emerged as a powerful technique for image synthesis [11; 16; 47], achieving state-of-the-art performance in various applications [13; 29; 15]. Among them, text-to-image diffusion models have garnered significant attention and witnessed a surge in demand [41; 38; 37]. Traditionally, diffusion models have adhered to the typical deep learning approach of training and testing on images with predetermined sizes, which generally leads to high-quality results. They still exhibit a range of visual defects and diverse flaws when confronted with a novel synthesizing resolution (e.g., 512^2 in training while 224^2 in testing). However, real-world scenarios often demand the generation of images with diverse sizes and aspect ratios, necessitating models that can handle such variety with minimum loss in visual fidelity. The necessity becomes even more severe in the generation of large models. As the size of models continues to increase, the associated training costs experience a substantial surge, thereby posing financial challenges for average programmers and emerging startups, making it unfeasible for them to train specialized models tailored to their specific needs. Consequently, there is an urgent demand to explore methodologies that facilitate the full utilization of open-sourced models trained on fixed sizes.

In regard to this limitation, our first key observation reveals that most instances of poor performance could be attributed to two prevalent patterns: **incomplete or inadequately represented objects** and

*Corresponding author

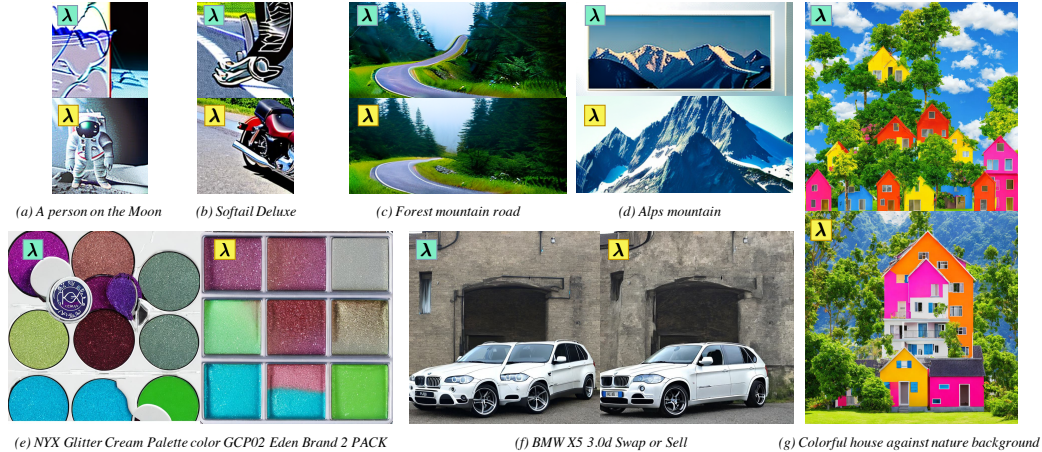


Figure 1: **Synthesized results** with the proposed scaling factor (marked with yellow icons) and those with original scaling factor (marked with green icons). The method with our scaling factor successfully synthesizes high-fidelity and natural images for different resolutions. Please zoom in for better visual effect.

repetitively disordered presentations. We have included several examples of flawed synthesized images in Figure 1, designated by green icons. Note that smaller images (e.g., images (a), (b), (c) and (d)) conform to the first pattern, showcasing inadequately depicted objects. Conversely, larger images (e.g., images (e), (f) and (g)) exhibit the second pattern, generating disordered objects in a repetitive manner. This delineation, also observed in other problematic cases, allows us to formulate our second key observation, where **lower resolution images are more vulnerable to the first pattern, while susceptibility to the second pattern increases in higher resolution images.**

In this work, we tackle the challenge of adapting text-to-image diffusion models to proficiently synthesize images spanning a wide range of sizes, encompassing both low and high resolutions. Our goal is threefold: (1) achieve a higher level of fidelity regardless of synthesized image resolutions; (2) mitigate the abovementioned two patterns; and (3) augment the semantic alignment between the synthesized images and the text prompts.

To accomplish these, our approach centers around the concept of entropy, which measures the spatial granularity of information aggregation. Specifically, when the attention entropy rises, each token is attending to wider spatial information, otherwise the opposite. Bearing that in mind, we establish the statistical relationship between the resolution (the number of tokens) and the entropy of attention maps. Our finding signifies that the attention entropy varies in correspondence with the quantity of tokens, which implies that models are aggregating spatial information in proportion to resolutions. We then establish our key interpretations based on the proportionality. In particular, since narrower attention is paid during the synthesis of low resolution images, models encounter difficulties in representing complete objects with limited spatial information. Conversely, when synthesizing high resolution images, each token tends to conduct a wide spatial aggregation which results in a redundancy of analogous spatial information and the disordered presentations of repeated elements.

Based on the statistical relationship and interpretations, we propose a novel scaling factor specifically designed for mitigating the change of the entropy in visual attention layers. We conduct qualitative and quantitative experiments to validate the efficacy of our scaling factor, which synthesizes results of varied resolutions with better visual effect and achieves better scores in image quality and text alignment. It is worth noting that the improvement is implemented in a training-free manner by replacing a single scaling factor in the attention layers.

The contributions are summarized as follows:

- We observe two distinct patterns of defects that low resolution images are prone to impaired object portrayal while repetitively disordered presentation exhibits in high resolution images.
- We establish a statistical relationship between attention the entropy and the resolution, which interprets the patterns by ascribing them to the lack or the surplus of the spatial information.

- We propose a scaling factor to efficiently improve variable-sized text-to-image synthesis in a training-free manner. We conduct various experiments and analysis to validate the efficacy.

2 Related Work

Image super-resolution and extrapolation. An alternative path to generate new images with different resolutions is post-processing synthesized images with image super-resolution and extrapolation methods. Super-resolution methods [19; 7; 54; 55] dedicate to exploiting the high frequency information of images and extending both the height and width of images by a fixed factor, which cannot change the aspect ratio of images. For extrapolation methods, they do have the ability to change the aspect ratio by extending images beyond their boundaries [51; 59; 30]. However, these methods are effective for signals that exhibit an intensive stationary component [6] (e.g., landscapes) while we would like to generate images with various scenes. Additionally, extrapolation methods might have discrepancy with diffusion models, resulting in inharmonious visual effect. Instead of adding more methods for post-processing and making the pipeline lengthy, we seek to synthesize high-fidelity images with diffusion models alone.

Diffusion models and attention mechanism. Diffusion models have emerged as a promising family of deep generative models with outstanding performance in image synthesis [11; 16; 23; 46; 47; 48]. They have significantly revolutionized computer vision research in multiple areas, including image editing [9; 13; 32], inpainting [29; 40; 57], super-resolution [17; 42] and video synthesis [15; 18]. These models generate high-quality images by smoothly denoising a noisy image sampled from a standard Gaussian distribution through multiple iterations. A key component in diffusion models is the attention module. Previous works such as denoising diffusion probabilistic model [16], denoising diffusion implicit model [47], latent diffusion model [38] have demonstrated the capability empowered by the attention modules. Note that attention modules in diffusion models are dealing with thousands of visual tokens and one of the most well-known research concern of attention is how to lower its conventional quadratic complexity against the large token numbers. To deal with this, most works define a sparse attention pattern to restrict each query to attend to a limited subset of tokens exclusively. The sparse attention pattern could be either defined as fixed windows [24; 53; 50; 39; 31] or learned during training [26; 35; 8; 5; 1; 61; 27; 58; 56; 10; 21]. We draw upon the insights in these works for sparsity controlling and seek to efficiently adapt trained models for variable-sized data.

Attention entropy. Introduced in the information theory by [45], entropy serves as a measure for information and uncertainty. Different research works have introduced entropy to attention maps in various tasks, including semantic segmentation [25], text classification [2], text generation [49], active visual exploration [34] and interpretability analysis [33]. Among them, the work in text generation [49] closely aligns with ours on attention scaling, leveraging Transformers to accommodate sentences of variable lengths. We draw upon the innovations in the entropy of attention maps for information quantification and seek to exploit both of its practicability and interpretability.

3 Method

This section establishes the connection between the attention entropy and the token number in a statistical manner and presents a scaling factor replaced into diffusion model for variable-sized image synthesis. Our aim is to alleviate the fluctuation in attention entropy with varying token numbers.

3.1 Connection: the attention entropy and the token number

Diffusion models refer to probabilistic models that learn a data distribution by iteratively refining a normally distributed variable, which is equivalent to learn the reverse process of a fixed Markov Chain with a length of T . In image synthesis, the most efficacious models make use of a Transformer-based encoder-decoder architecture for the denoising step. This step can be understood as an evenly weighted chain of denoising autoencoders, which are trained to predict a filtered version of their input via cross-attention. Yet the scaling factor inside the attention module of diffusion models is so far an under-explored area of research. In this section, we focus on enhancing conditional diffusion models by adaptively determining the scaling factor of Transformer encoder-decoder backbones.

Let $\mathbf{X} \in \mathbb{R}^{N \times d}$ denotes an image token sequence to an attention module, where N, d are the number of tokens and the token dimension, respectively. We then denote the key, query and value matrices as $\mathbf{K} = \mathbf{X}\mathbf{W}^K, \mathbf{Q}$ and \mathbf{V} , where $\mathbf{W}^K \in \mathbb{R}^{d \times d_r}$ is a learnable projection matrix and d_r is the projection dimension. The attention layer ([3; 52]) computes $\text{Attention}(\mathbf{Q}, \mathbf{K}, \mathbf{V}) = \mathbf{A}\mathbf{V}$ with the attention map \mathbf{A} calculated by the row-wise softmax function as follows:

$$\mathbf{A}_{i,j} = \frac{e^{\lambda \mathbf{Q}_i \mathbf{K}_j^\top}}{\sum_{j'=1}^N e^{\lambda \mathbf{Q}_i \mathbf{K}_{j'}^\top}}, \quad (1)$$

where λ is a scaling factor, usually set as $1/\sqrt{d}$ in the widely-used Scaled Dot-Product Attention [52] and i, j are the row indices on the matrices \mathbf{Q} and \mathbf{K} , respectively. Following [2; 12], we calculate the attention entropy by treating the attention distribution of each token as a probability mass function of a discrete random variable. The attention entropy with respect to the i^{th} row of \mathbf{A} is defined as:

$$\text{Ent}(\mathbf{A}_i) = - \sum_{j=1}^N \mathbf{A}_{i,j} \log(\mathbf{A}_{i,j}), \quad (2)$$

where the attention entropy gets its maximum when $\mathbf{A}_{i,j} = 1/N$ for all j and gets its minimum when $\mathbf{A}_{i,j'} = 1$ and $\mathbf{A}_{i,j} = 0$ for any $j \neq j'$. It implies that the attention entropy measures the spatial granularity of information aggregation. A larger attention entropy suggests that wider contextual information is taken into account while a smaller entropy indicates only few tokens are weighed.

We now investigate the relation between the attention entropy and the token number. By substituting Eq.(1) into Eq.(2), we have:

$$\begin{aligned} \text{Ent}(\mathbf{A}_i) &= - \sum_{j=1}^N \left[\frac{e^{\lambda \mathbf{Q}_i \mathbf{K}_j^\top}}{\sum_{j'=1}^N e^{\lambda \mathbf{Q}_i \mathbf{K}_{j'}^\top}} \log \left(\frac{e^{\lambda \mathbf{Q}_i \mathbf{K}_j^\top}}{\sum_{j'=1}^N e^{\lambda \mathbf{Q}_i \mathbf{K}_{j'}^\top}} \right) \right] \\ &\approx \log N + \log \mathbb{E}_j(e^{\lambda \mathbf{Q}_i \mathbf{K}_j^\top}) - \frac{\mathbb{E}_j(\lambda \mathbf{Q}_i \mathbf{K}_j^\top e^{\lambda \mathbf{Q}_i \mathbf{K}_j^\top})}{\mathbb{E}_j(e^{\lambda \mathbf{Q}_i \mathbf{K}_j^\top})}, \end{aligned} \quad (3)$$

where \mathbb{E}_j denotes the expectation upon the index j , and the last equality holds asymptotically when N gets larger. For the complete proof, please refer to the Supplementary Materials.

Given \mathbf{X} as an encoded sequence from an image, each token \mathbf{X}_j could be assumed as a vector sampled from a multivariate Gaussian distribution $\mathcal{N}(\boldsymbol{\mu}^X, \boldsymbol{\Sigma}^X)$. This prevailing assumption is widely shared in the fields of image synthesis [14] and style transfer [20; 28; 22]. In this way, each $\mathbf{K}_j = \mathbf{X}_j \mathbf{W}^K$ could be considered as a sample from the multivariate Gaussian distribution $\mathcal{N}(\boldsymbol{\mu}^K, \boldsymbol{\Sigma}^K) = \mathcal{N}(\boldsymbol{\mu}^X \mathbf{W}^K, (\mathbf{W}^K)^\top \boldsymbol{\Sigma}^X \mathbf{W}^K)$. In regard to \mathbf{K}_j , its dimension-wise linear combination $y_i = \lambda \mathbf{Q}_i \mathbf{K}_j^\top$ could be treated as a scalar random variable sampled from the univariate Gaussian distribution $y_i \sim \mathcal{N}(\mu_i, \sigma_i^2) = \mathcal{N}(\lambda \mathbf{Q}_i (\boldsymbol{\mu}^K)^\top, \lambda^2 \mathbf{Q}_i \boldsymbol{\Sigma}^K \mathbf{Q}_i^\top)$. Under this circumstance, we dive into the expectations $\mathbb{E}_j(e^{\lambda \mathbf{Q}_i \mathbf{K}_j^\top})$ and $\mathbb{E}_j(\lambda \mathbf{Q}_i \mathbf{K}_j^\top e^{\lambda \mathbf{Q}_i \mathbf{K}_j^\top})$ in Eq.(3):

$$\begin{aligned} \mathbb{E}_j(e^{\lambda \mathbf{Q}_i \mathbf{K}_j^\top}) &\doteq \mathbb{E}_j(e^{y_i}) = e^{\mu_i + \frac{\sigma_i^2}{2}} \\ \mathbb{E}_j(\lambda \mathbf{Q}_i \mathbf{K}_j^\top e^{\lambda \mathbf{Q}_i \mathbf{K}_j^\top}) &\doteq \mathbb{E}_j(y_i e^{y_i}) = (\mu_i + \sigma_i^2) e^{\mu_i + \frac{\sigma_i^2}{2}}, \end{aligned} \quad (4)$$

For the complete proof, please refer to the Supplementary Materials. By substituting Eq.(4) into Eq.(3), we have:

$$\begin{aligned} \text{Ent}(\mathbf{A}_i) &= \log N + \log \left(e^{\mu_i + \frac{\sigma_i^2}{2}} \right) - \frac{(\mu_i + \sigma_i^2) e^{\mu_i + \frac{\sigma_i^2}{2}}}{e^{\mu_i + \frac{\sigma_i^2}{2}}} \\ &= \log N - \frac{\sigma_i^2}{2}. \end{aligned} \quad (5)$$

The observation is that the attention entropy varies correspondingly with N in a logarithm magnitude while the latter item $\sigma_i^2 = \lambda^2 \mathbf{Q}_i \boldsymbol{\Sigma}^K \mathbf{Q}_i^\top$ is not relevant with the token number N in the setting of images generation. This implies that each token intends to adaptively deal with wider contextual information for higher resolutions, and narrower contextual information for lower resolutions.

Interpretations on two observed patterns. Our key insight lies in the correlation between the fluctuating attention entropy and the emergence of two defective patterns in our observations. Specifically, when the model is synthesizing images with lower resolutions, the attention entropy experiences a statistical decline of $\log N$, leading to a reduced attention on contextual information. Consequently, each token is processing discrete information in isolation and the model struggles to generate objects with intricate details and smooth transitions, giving rise to the first observed pattern.

Conversely, in scenarios involving higher resolutions, the attention entropy exhibits an upward trend, accompanied by the utilization of overwhelming amounts of global information for synthesis. Consequently, each token is processing analogous information and the model generates repetitively disordered presentations, exemplifying the second pattern.

3.2 A scaling factor for mitigating entropy fluctuations

To alleviate the fluctuating entropy with respect to different token numbers N in the inference phase, considering the quadratic form in Eq.(5), we set the scaling hyper-parameter λ in the following form:

$$\lambda = c\sqrt{\log N}, \tag{6}$$

where c denotes a constant number. Note that when the token number N is set as the number of tokens during training (denoted as T), λ should specialize to $1/\sqrt{d}$ for the best stabilization of entropy (i.e., $c\sqrt{\log T} \approx 1/\sqrt{d}$). Thus, we have an approximate value of c and substitute it into Eq.(6):

$$\lambda \approx \sqrt{\frac{1}{d \log T}} \cdot \sqrt{\log N} = \sqrt{\frac{\log_T N}{d}}. \tag{7}$$

Intuitively, if the model is dealing with a token number $N > T$, the proposed scaling factor would multiply the feature maps by a factor of squared $\log_T N$ to maintain the rising entropy, and vice versa. Thus, the proposed scaling factor is implemented in a training-free manner, which enjoys better performances in synthesizing images of different resolutions. The illustration of our proposed method is shown in Figure 2.

4 Experimental Results

In this section, we evaluate our proposed method on text-to-image synthesis and analyse the efficacy of the proposed scaling factor. The quantitative and qualitative results demonstrate a better performance of our scaling factor. Please refer to the Supplemental Materials for detailed experimental results.

4.1 Text-to-image synthesis

Experimental setup. We explore the adapting ability of the proposed scaling factor for diffusion models in variable-sized text-to-image synthesis. In particular, we replace the scaling factor of self-attention layers within diffusion models and evaluate their performance without any training upon a subset of LAION-400M and LAION-5B dataset ([44; 43]), which contain over 400 million and 5.85 billion CLIP-filtered image-text pairs, respectively. We randomly choose text-image pairs out from each dataset and generate images corresponding to texts in multiple settings for evaluation. As for the diffusion models, we consider both Stable Diffusion [38] trained on LAION-5B and Latent Diffusion [38] trained on LAION-400M to test the performances. The former (which is set to synthesize images with a 512×512 resolution by default) maintains 4x longer sequences compared with the latter (with a default 256×256 resolution) across all the layers. For more evaluation results and details, please refer to the Supplementary Materials.

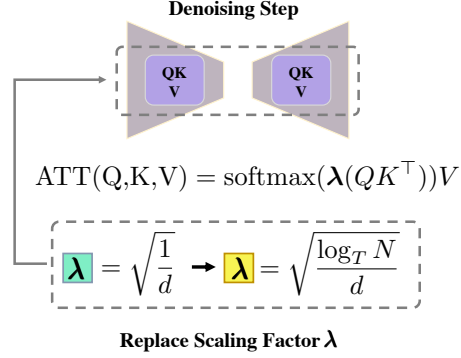


Figure 2: The illustration of our proposed process of replacing the scaling factor without additional training, where T and N denote the number of tokens in the training phase and the inference phase.

Table 1: **FID scores** (\downarrow) for Stable Diffusion and Latent Diffusion in different resolution settings. Stable Diffusion scores 19.8168 for default 512² and Latent Diffusion scores 20.4102 for default 256².

Stable Diffusion - 512			Latent Diffusion - 256		
Resolution	Original	Ours	Resolution	Original	Ours
224 * 224	74.5742	41.8925	128 * 128	65.2988	57.5542
448 * 448	19.9039	19.4923	224 * 224	23.0483	22.7971
768 * 768	29.5974	28.1372	384 * 384	20.5466	20.3842
512 * 288	22.6249	21.3877	256 * 144	33.8559	33.0142
512 * 384	20.2315	19.8631	256 * 192	24.2546	23.9346

Table 2: **CLIP scores** (\uparrow) for Stable Diffusion and Latent Diffusion in different resolution settings. Stable Diffusion scores 0.3158 for default 512² and Latent Diffusion scores 0.3153 for default 256².

Stable Diffusion - 512			Latent Diffusion - 256		
Resolution	Original	Ours	Resolution	Original	Ours
224 * 224	0.2553	0.2764	128 * 128	0.2679	0.2747
448 * 448	0.3176	0.3180	224 * 224	0.3094	0.3096
768 * 768	0.3142	0.3152	384 * 384	0.3148	0.3156
512 * 288	0.3047	0.3066	256 * 144	0.2884	0.2890
512 * 384	0.3134	0.3139	256 * 192	0.3070	0.3075

Table 3: **Results of human evaluation.** We report the score of consistency (\uparrow) for the text-to-image results of Stable Diffusion in different resolution settings.

Resolution	224 * 224	448 * 448	768 * 768	512 * 288	512 * 384
Original	5.13	6.45	6.74	6.11	6.75
Ours	6.77	7.12	7.56	7.42	6.98

Quantitative comparison. We compare the performance of the proposed scaling factor against the scaling factor $\lambda = 1/\sqrt{d}$ for Stable Diffusion [38] and Latent Diffusion [38] in multiple squared resolution settings (small, medium and large sizes according to their default training sizes). We evaluate them with the metric of Fréchet Inception Distance (FID) [14], which measures image quality and diversity. As shown in Table 1, our scaling factor universally improves FID for both Stable Diffusion and Latent Diffusion in all resolution settings, especially for the images with small resolution (a significant improvement from 74.6 to 41.9 for Stable Diffusion on the resolution 224 × 224). It is worth noting that the proposed method needs no additional training and achieves these in a plug-and-play manner with trivial complexity.

Besides FID, we also evaluate the degree of semantic alignment between text prompts and the corresponding synthesized images with CLIP scores [36], which utilizes contrastive learning to establish connections between visual concepts and natural language concepts. As shown in Table 2, our scaling factor achieves better CLIP scores than the original one in all resolution settings. It shows that our scaling factor performs better in the alignment of text prompts and the synthesized images.

Additionally, we present the results of user study in Table 3. We conduct a text-based pairwise preference test. That is, for a given sentence, we pair the image from our model with the synthesized image from the baseline model and ask 45 annotators in total to give each synthesized image a rating score for consistency. For each human annotators, we pay \$15 for effective completeness of user study evaluation. We observe that users rate higher for our method, which suggests that the synthesized images from our method are more contextually coherent with texts than the baseline. Besides, with the refinement from the proposed scaling factor, the generated contents from our model are able to convey more natural and informative objects.

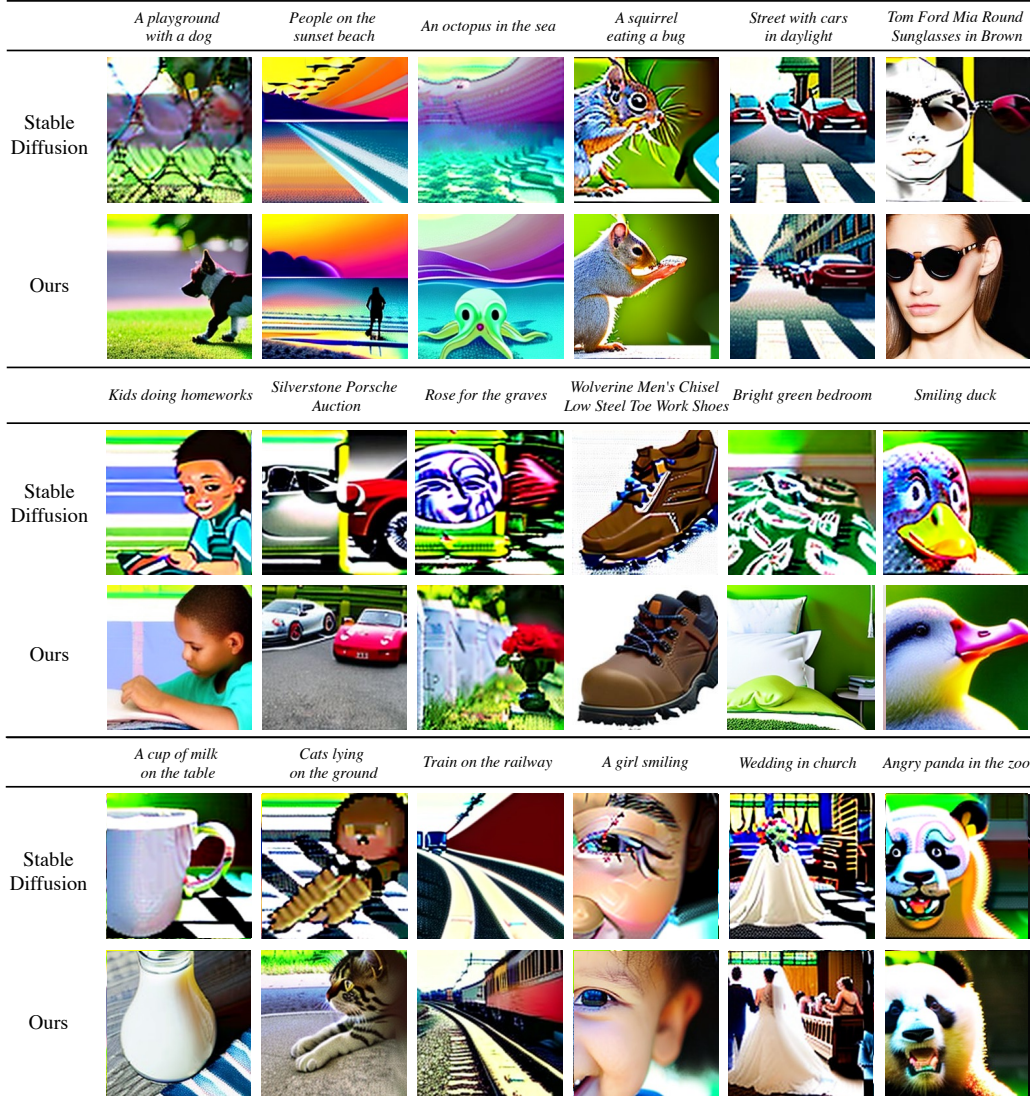


Figure 3: **Qualitative comparison** on the scale factors for the resolution 224×224 . The original scaling factor misses out content or roughly depicts the objects in prompts while our scaling factor manages to synthesize visual concepts in high fidelity and better illumination. Please zoom in for better visual effect.

Qualitative comparison. In Figures 3 and 4, we show some visualization results for the qualitative comparison between two scaling factors with Stable Diffusion. Paired images are synthesized with the same seeds and text prompts. Please zoom in for the best visual effect. For Figure 3, we demonstrate results under the proposed and the original scaling factors for Stable Diffusion with 224×224 resolution, which is lower than the default training resolution 512×512 of Stable Diffusion. We observe that in the original Stable Diffusion setting, objects are either missed out (e.g., absent dog, people and octopus) or roughly depicted (e.g., crudely rendered squirrel, cars and person with sunglasses). Our interpretation is that for lower resolutions, according to Eq. (5), the model is synthesizing images with a less entropy during the inference phase when compared to its training phase, which implies that the model is suffering from deprived information. In this way, the model has more difficulty in generating complex objects and cannot generate attractive images. As for the results generated by the proposed scaling factor, we show that images are synthesized with better alignments with prompts (e.g., clear presence of dog, people and octopus) and objects are generated more vividly (e.g., realistic squirrel, cars and person with sunglasses). Note that our scaling factor also performs better in the illumination and shading because of the utilization of more aggregated

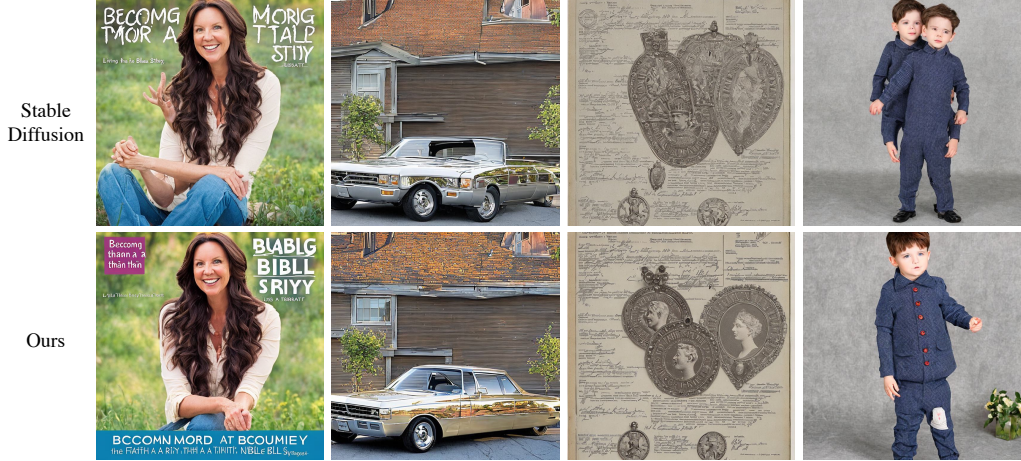


Figure 4: **Qualitative comparison** on the scale factors for the resolution 768×768 . The original scaling factor generates objects in repeated and messy patterns while our scaling factor manages to spatially arrange the visual concepts in clear order. Please zoom in for better visual effect.

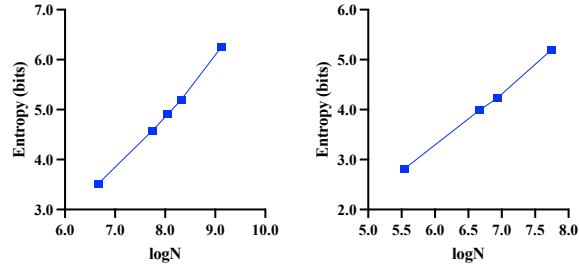


Figure 5: **Analysis results** on the average attention entropy with respect to the number of tokens for Stable Diffusion model (left) and latent diffusion model (right). N refers to the number of tokens. As shown in the figure, average attention entropy has a linear relationship with the logarithm of N , which confirms the effectiveness of our asymptotic equality in Eq.(5)

and contextualized information with higher entropy. Considering its flexibility, our method might offer valuable insights into the fields of inpainting [29; 57] and compositional scene generation [60].

For Figure 4, we demonstrate the results of Stable Diffusion under the proposed and the original scaling factors with the 768×768 resolution, which is higher than the default training resolution 512×512 of Stable Diffusion. Different from the rough objects in Figure 3, we note that objects are depicted with overwhelming details in a messy and disordered manner (e.g., repeated hands, a extended vehicle and messy seals). The reason is that for higher resolutions, according to Eq.(5), the model are bearing more entropy than it does in the training period. As a result, tokens are attending to numerous but redundant global information and the model depicts objects with burdensome details, leading to the patterns observed. For the results by our scaling factor, we note that the repeated patterns are greatly alleviated (e.g., a pair of normal hands and a regular vehicle) and synthesized objects are spatially arranged in order without losing the details (three seals well depicted in order).

4.2 Analysis

In this section, we conduct a comprehensive analysis of the practical implications of our theoretical findings. This analysis is of great importance due to the nature of our fundamental theoretical discovery outlined in Eq.(5). As an asymptotic equality, it might exhibit limitations in practical scenarios where the token quantity, denoted as N , falls below a certain threshold. Thus, it becomes imperative to assess the feasibility and the applicability of our theoretical finding under such circumstances. Subsequently, we delve into an in-depth examination of the pivotal role played by the scaling factor

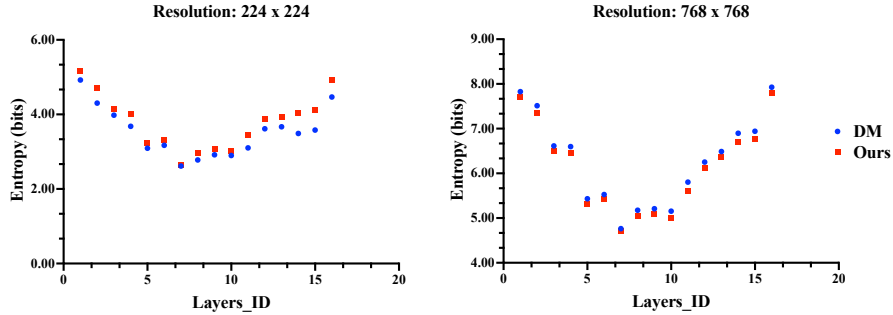


Figure 6: **Analysis results** on the average attention entropy with respect to two scale factors for two resolution. Layer ID refers to the index number of self-attention layers in the model and DM stands for original diffusion model. The figure illustrate that the proposed scaling factor mitigates the fluctuation of attention entropy.

in mitigating the fluctuations within the attention entropy, as presented in Section 3.2. This rigorous analysis serves to substantiate and validate the insights elucidated in the aforementioned section. To support our claims, we present visually intuitive representations of the empirical results, which unequivocally demonstrate the alignment between our statements and the experimental outcomes.

The relationship between the attention entropy and the token number. We conduct an experiment on text-to-image tasks to investigate the relation between the entropy and the token number N , which is statistically connected in Eq.(5). In particular, we synthesize images with various resolutions (including 224^2 , 384^2 , 448^2 , 512^2 and 768^2 for Stable Diffusion and 128^2 , 224^2 , 256^2 and 384^2 for Latent Diffusion model) and calculate their attention entropy during the inference period. We average the results across attention heads and layers for 5K samples on each resolution. Figure 5 illustrates that the average attention entropy has a linear relationship with the logarithm of the quantity of tokens for both diffusion models, which accords with their asymptotic relationship proposed in Eq.(5). The visualized results provide the empirical evidence that substantiates the efficacy of our theoretical findings and the feasible extensions for those resolutions close to the mentioned resolutions.

The role of scaling factor for stabilizing the attention entropy. We conduct an experiment on the mitigating effect of the proposed scaling factor onto the fluctuated attention entropy. Specifically, with two scaling factors, we synthesize images with a lower and a higher resolution (including 224^2 and 768^2 for Stable Diffusion) and record their attention entropy for each attention layers. We average the results across attention heads for 5K samples. As demonstrated in the Figure 6, the proposed scaling factor does contribute to an increase in the synthesis process for the resolution 224^2 and a decrease in that for the resolution 768^2 , which accords with our motivation in Section 3.2 and shows the efficacy of our scaling factor in mitigating the fluctuation of the attention entropy.

4.3 Difference with other candidate methods

In this section, we discuss upon the difference between the proposed method and other candidate methods for variable-sized image synthesis, including up/down-sampling methods and super-resolution methods. While all the mentioned methods share the same goal to synthesis images of variable sizes, there are three distinctive features setting our method apart from the rest.

Different aspect ratio. Other candidate methods do not support diffusion models to generate new images with a different aspect ratio. In comparison, our method could improve image synthesis in different aspect ratio, validated by both qualitative and quantitative experiments in Section 4.1.

Richness of visual information (important for higher resolutions). When users generate images with higher resolutions, what they are expecting is not only more pixels but also richer semantic information in images. Under this circumstance, our method augments semantic information by enabling models to deal with more tokens in an adaptive manner, which enables images to possess a more extensive range of content. As shown in Figure 7, our method generates images with more

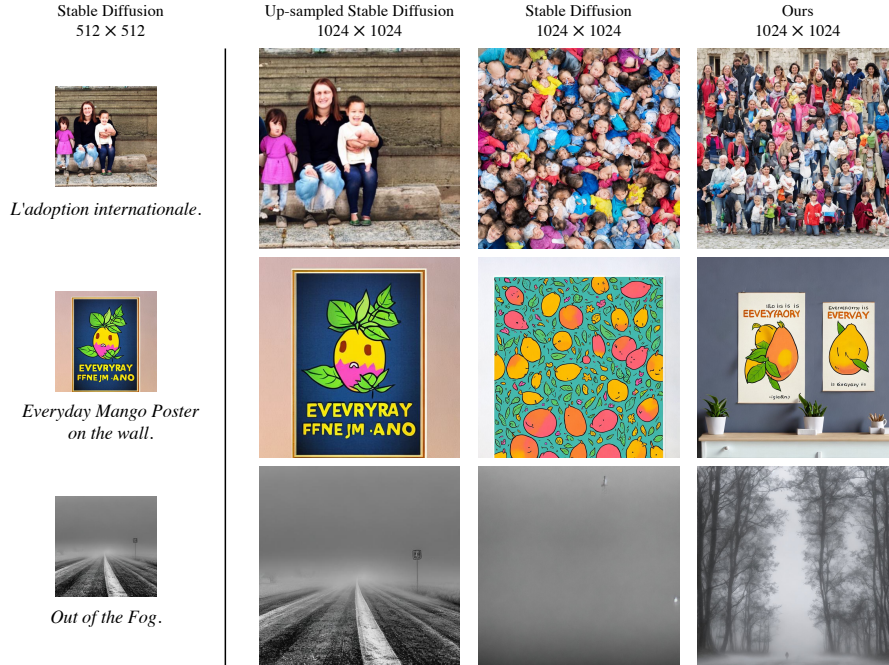


Figure 7: **Qualitative results** to illustrate the difference in visual information richness between up-sampled methods, the original Stable Diffusion and the proposed method. Note that our method (right) introduces more visual information with a different level of granularity compared with up-sampling and super-resolution methods (left). Additionally, our method could better deal with repetitively disordered pattern emerging in the original Stable Diffusion model (middle).

richness and expressiveness in semantics. In contrast, super-resolution and other methods scale up the original images and focus on better image clarity and finer details instead of richer semantics, introducing visual information at a different granularity level compared with the proposed method.

Time cost and memory usage (important for lower resolutions). For diffusion models adapted by our method, their time cost and spatial usage become proportional to the generation resolution, while down-sampling methods are constantly constrained to the fixed cost brought by training resolutions. As a result, our method could efficiently enable low resolution image synthesis especially on portable devices, which has a high demand for both time cost and memory usage other than image fidelity. For more quantitative results to support this, please refer to the Supplementary Materials.

5 Conclusion

In this work, we delve into a new perspective of adapting diffusion models to effectively synthesize images of varying sizes with superior visual quality, based on the concept of entropy. We establish a statistical connection between the number of tokens and the entropy of attention maps. Utilizing this connection, we give interpretations to the defective patterns we observe and propose a novel scaling factor for visual attention layers to better handle sequences of varying lengths. The experimental results demonstrate that our scaling factor effectively enhances both quantitative and qualitative scores for text-to-image of varying sizes in a training-free manner, while stabilizing the entropy of attention maps for variable token numbers. Moreover, we provide extensive analysis and discussion for the efficiency and the significance of our method.

Limitations One limitation of this study pertains to the metrics used for quantitative evaluation. While these metrics primarily evaluate the quality of the generated content, there is a lack of methodology for evaluating the fidelity of images for different resolutions. The same issue applies for the evaluation of repetitively disordered pattern, which is in part compensated by qualitative scores.

Acknowledgment

This work was supported in part by the National Key R&D Program of China (No.2021ZD0112803), the National Natural Science Foundation of China (No.62176060, No.62176061), STCSM project (No.22511105000), Shanghai Municipal Science and Technology Major Project (2021SHZDZX0103), UniDT’s Cognitive Computing and Few Shot Learning Project, and the Program for Professor of Special Appointment (Eastern Scholar) at Shanghai Institutions of Higher Learning.

References

- [1] Joshua Ainslie, Santiago Ontanon, Chris Alberti, Vaclav Cvicek, Zachary Fisher, Philip Pham, Anirudh Ravula, Sumit Sanghai, Qifan Wang, and Li Yang. Etc: Encoding long and structured inputs in transformers. *arXiv preprint arXiv:2004.08483*, 2020.
- [2] Giuseppe Attanasio, Debora Nozza, Dirk Hovy, and Elena Baralis. Entropy-based attention regularization frees unintended bias mitigation from lists. *arXiv preprint arXiv:2203.09192*, 2022.
- [3] Dzmitry Bahdanau, Kyunghyun Cho, and Yoshua Bengio. Neural machine translation by jointly learning to align and translate. *arXiv preprint arXiv:1409.0473*, 2014.
- [4] Omer Bar-Tal, Lior Yariv, Yaron Lipman, and Tali Dekel. Multidiffusion: Fusing diffusion paths for controlled image generation. 2023.
- [5] Iz Beltagy, Matthew E Peters, and Arman Cohan. Longformer: The long-document transformer. *arXiv preprint arXiv:2004.05150*, 2020.
- [6] Lucy Chai, Michael Gharbi, Eli Shechtman, Phillip Isola, and Richard Zhang. Any-resolution training for high-resolution image synthesis. In *Computer Vision—ECCV 2022: 17th European Conference, Tel Aviv, Israel, October 23–27, 2022, Proceedings, Part XVI*, pages 170–188. Springer, 2022.
- [7] Yinbo Chen, Sifei Liu, and Xiaolong Wang. Learning continuous image representation with local implicit image function. In *Proceedings of the IEEE/CVF conference on computer vision and pattern recognition*, pages 8628–8638, 2021.
- [8] Rewon Child, Scott Gray, Alec Radford, and Ilya Sutskever. Generating long sequences with sparse transformers. *arXiv preprint arXiv:1904.10509*, 2019.
- [9] Guillaume Couairon, Jakob Verbeek, Holger Schwenk, and Matthieu Cord. Diffedit: Diffusion-based semantic image editing with mask guidance. *arXiv preprint arXiv:2210.11427*, 2022.
- [10] Tri Dao, Beidi Chen, Kaizhao Liang, Jiaming Yang, Zhao Song, Atri Rudra, and Christopher Re. Pixelated butterfly: Simple and efficient sparse training for neural network models. *arXiv preprint arXiv:2112.00029*, 2021.
- [11] Prafulla Dhariwal and Alexander Nichol. Diffusion models beat gans on image synthesis. *Advances in Neural Information Processing Systems*, 34:8780–8794, 2021.
- [12] Hamidreza Ghader and Christof Monz. What does attention in neural machine translation pay attention to? *arXiv preprint arXiv:1710.03348*, 2017.
- [13] Amir Hertz, Ron Mokady, Jay Tenenbaum, Kfir Aberman, Yael Pritch, and Daniel Cohen-Or. Prompt-to-prompt image editing with cross attention control. *arXiv preprint arXiv:2208.01626*, 2022.
- [14] Martin Heusel, Hubert Ramsauer, Thomas Unterthiner, Bernhard Nessler, and Sepp Hochreiter. Gans trained by a two time-scale update rule converge to a local nash equilibrium. *Advances in neural information processing systems*, 30, 2017.
- [15] Jonathan Ho, William Chan, Chitwan Saharia, Jay Whang, Ruiqi Gao, Alexey Gritsenko, Diederik P Kingma, Ben Poole, Mohammad Norouzi, David J Fleet, et al. Imagen video: High definition video generation with diffusion models. *arXiv preprint arXiv:2210.02303*, 2022.

- [16] Jonathan Ho, Ajay Jain, and Pieter Abbeel. Denoising diffusion probabilistic models. *Advances in Neural Information Processing Systems*, 33:6840–6851, 2020.
- [17] Jonathan Ho, Chitwan Saharia, William Chan, David J Fleet, Mohammad Norouzi, and Tim Salimans. Cascaded diffusion models for high fidelity image generation. *J. Mach. Learn. Res.*, 23(47):1–33, 2022.
- [18] Jonathan Ho, Tim Salimans, Alexey Gritsenko, William Chan, Mohammad Norouzi, and David J Fleet. Video diffusion models. *arXiv preprint arXiv:2204.03458*, 2022.
- [19] Xuecai Hu, Haoyuan Mu, Xiangyu Zhang, Zilei Wang, Tieniu Tan, and Jian Sun. Meta-sr: A magnification-arbitrary network for super-resolution. In *Proceedings of the IEEE/CVF conference on computer vision and pattern recognition*, pages 1575–1584, 2019.
- [20] Xun Huang and Serge Belongie. Arbitrary style transfer in real-time with adaptive instance normalization. In *Proceedings of the IEEE international conference on computer vision*, pages 1501–1510, 2017.
- [21] DeLesley Hutchins, Imanol Schlag, Yuhuai Wu, Ethan Dyer, and Behnam Neyshabur. Block-recurrent transformers. *arXiv preprint arXiv:2203.07852*, 2022.
- [22] Zhiyu Jin, Xuli Shen, Bin Li, and Xiangyang Xue. Style spectroscopy: Improve interpretability and controllability through fourier analysis. *arXiv preprint arXiv:2208.06140*, 2022.
- [23] Tero Karras, Miika Aittala, Timo Aila, and Samuli Laine. Elucidating the design space of diffusion-based generative models. *arXiv preprint arXiv:2206.00364*, 2022.
- [24] Nikita Kitaev, Łukasz Kaiser, and Anselm Levskaya. Reformer: The efficient transformer. *arXiv preprint arXiv:2001.04451*, 2020.
- [25] Krzysztof Lis, Matthias Rottmann, Sina Honari, Pascal Fua, and Mathieu Salzmann. Attentropy: Segmenting unknown objects in complex scenes using the spatial attention entropy of semantic segmentation transformers. *arXiv preprint arXiv:2212.14397*, 2022.
- [26] Peter J Liu, Mohammad Saleh, Etienne Pot, Ben Goodrich, Ryan Sepassi, Łukasz Kaiser, and Noam Shazeer. Generating wikipedia by summarizing long sequences. *arXiv preprint arXiv:1801.10198*, 2018.
- [27] Ze Liu, Yutong Lin, Yue Cao, Han Hu, Yixuan Wei, Zheng Zhang, Stephen Lin, and Baining Guo. Swin transformer: Hierarchical vision transformer using shifted windows. In *Proceedings of the IEEE/CVF international conference on computer vision*, pages 10012–10022, 2021.
- [28] Ming Lu, Hao Zhao, Anbang Yao, Yurong Chen, Feng Xu, and Li Zhang. A closed-form solution to universal style transfer. In *Proceedings of the IEEE/CVF International Conference on Computer Vision*, pages 5952–5961, 2019.
- [29] Andreas Lugmayr, Martin Danelljan, Andres Romero, Fisher Yu, Radu Timofte, and Luc Van Gool. Repaint: Inpainting using denoising diffusion probabilistic models. In *Proceedings of the IEEE/CVF Conference on Computer Vision and Pattern Recognition*, pages 11461–11471, 2022.
- [30] Ye Ma, Jin Ma, Min Zhou, Quan Chen, Tiezheng Ge, Yuning Jiang, and Tong Lin. Boosting image outpainting with semantic layout prediction. *arXiv preprint arXiv:2110.09267*, 2021.
- [31] Lovish Madaan, Srinadh Bhojanapalli, Himanshu Jain, and Prateek Jain. Treeformer: Dense gradient trees for efficient attention computation. *arXiv preprint arXiv:2208.09015*, 2022.
- [32] Chenlin Meng, Yutong He, Yang Song, Jiaming Song, Jiajun Wu, Jun-Yan Zhu, and Stefano Ermon. Sdedit: Guided image synthesis and editing with stochastic differential equations. In *International Conference on Learning Representations*, 2021.
- [33] Byung-Doh Oh and William Schuler. Entropy-and distance-based predictors from gpt-2 attention patterns predict reading times over and above gpt-2 surprisal. *arXiv preprint arXiv:2212.11185*, 2022.

- [34] Adam Pardyl, Grzegorz Rypeś, Grzegorz Kurzejamski, Bartosz Zieliński, and Tomasz Trzcinski. Active visual exploration based on attention-map entropy. *arXiv preprint arXiv:2303.06457*, 2023.
- [35] Niki Parmar, Ashish Vaswani, Jakob Uszkoreit, Lukasz Kaiser, Noam Shazeer, Alexander Ku, and Dustin Tran. Image transformer. In *International conference on machine learning*, pages 4055–4064. PMLR, 2018.
- [36] Alec Radford, Jong Wook Kim, Chris Hallacy, Aditya Ramesh, Gabriel Goh, Sandhini Agarwal, Girish Sastry, Amanda Askell, Pamela Mishkin, Jack Clark, et al. Learning transferable visual models from natural language supervision. In *International conference on machine learning*, pages 8748–8763. PMLR, 2021.
- [37] Aditya Ramesh, Prafulla Dhariwal, Alex Nichol, Casey Chu, and Mark Chen. Hierarchical text-conditional image generation with clip latents. *arXiv preprint arXiv:2204.06125*, 2022.
- [38] Robin Rombach, Andreas Blattmann, Dominik Lorenz, Patrick Esser, and Björn Ommer. High-resolution image synthesis with latent diffusion models. In *Proceedings of the IEEE/CVF Conference on Computer Vision and Pattern Recognition*, pages 10684–10695, 2022.
- [39] Aurko Roy, Mohammad Saffar, Ashish Vaswani, and David Grangier. Efficient content-based sparse attention with routing transformers. *Transactions of the Association for Computational Linguistics*, 9:53–68, 2021.
- [40] Chitwan Saharia, William Chan, Huiwen Chang, Chris Lee, Jonathan Ho, Tim Salimans, David Fleet, and Mohammad Norouzi. Palette: Image-to-image diffusion models. In *ACM SIGGRAPH 2022 Conference Proceedings*, pages 1–10, 2022.
- [41] Chitwan Saharia, William Chan, Saurabh Saxena, Lala Li, Jay Whang, Emily L Denton, Kamyar Ghasemipour, Raphael Gontijo Lopes, Burcu Karagol Ayan, Tim Salimans, et al. Photorealistic text-to-image diffusion models with deep language understanding. *Advances in Neural Information Processing Systems*, 35:36479–36494, 2022.
- [42] Chitwan Saharia, Jonathan Ho, William Chan, Tim Salimans, David J Fleet, and Mohammad Norouzi. Image super-resolution via iterative refinement. *IEEE Transactions on Pattern Analysis and Machine Intelligence*, 2022.
- [43] Christoph Schuhmann, Romain Beaumont, Richard Vencu, Cade Gordon, Ross Wightman, Mehdi Cherti, Theo Coombes, Aarush Katta, Clayton Mullis, Mitchell Wortsman, et al. Laion-5b: An open large-scale dataset for training next generation image-text models. *arXiv preprint arXiv:2210.08402*, 2022.
- [44] Christoph Schuhmann, Richard Vencu, Romain Beaumont, Robert Kaczmarczyk, Clayton Mullis, Aarush Katta, Theo Coombes, Jenia Jitsev, and Aran Komatsuzaki. Laion-400m: Open dataset of clip-filtered 400 million image-text pairs. *arXiv preprint arXiv:2111.02114*, 2021.
- [45] C. E. Shannon. A mathematical theory of communication. *The Bell System Technical Journal*, 27(3):379–423, 1948.
- [46] Jascha Sohl-Dickstein, Eric Weiss, Niru Maheswaranathan, and Surya Ganguli. Deep unsupervised learning using nonequilibrium thermodynamics. In *International Conference on Machine Learning*, pages 2256–2265. PMLR, 2015.
- [47] Jiaming Song, Chenlin Meng, and Stefano Ermon. Denoising diffusion implicit models. *arXiv preprint arXiv:2010.02502*, 2020.
- [48] Yang Song, Jascha Sohl-Dickstein, Diederik P Kingma, Abhishek Kumar, Stefano Ermon, and Ben Poole. Score-based generative modeling through stochastic differential equations. *arXiv preprint arXiv:2011.13456*, 2020.
- [49] Jianlin Su. Revisiting attention scale operation from the invariance of entropy, Dec 2021. [Blog post]. Retrieved from <https://kexue.fm/archives/8823>.

- [50] Yi Tay, Dara Bahri, Liu Yang, Donald Metzler, and Da-Cheng Juan. Sparse sinkhorn attention. In *International Conference on Machine Learning*, pages 9438–9447. PMLR, 2020.
- [51] Piotr Teterwak, Aaron Sarna, Dilip Krishnan, Aaron Maschinot, David Belanger, Ce Liu, and William T Freeman. Boundless: Generative adversarial networks for image extension. In *Proceedings of the IEEE/CVF International Conference on Computer Vision*, pages 10521–10530, 2019.
- [52] Ashish Vaswani, Noam Shazeer, Niki Parmar, Jakob Uszkoreit, Llion Jones, Aidan N Gomez, Lukasz Kaiser, and Illia Polosukhin. Attention is all you need. *Advances in neural information processing systems*, 30, 2017.
- [53] Apoorv Vyas, Angelos Katharopoulos, and François Fleuret. Fast transformers with clustered attention. *Advances in Neural Information Processing Systems*, 33:21665–21674, 2020.
- [54] Xintao Wang, Liangbin Xie, Chao Dong, and Ying Shan. Real-esrgan: Training real-world blind super-resolution with pure synthetic data. In *Proceedings of the IEEE/CVF International Conference on Computer Vision*, pages 1905–1914, 2021.
- [55] Xintao Wang, Ke Yu, Shixiang Wu, Jinjin Gu, Yihao Liu, Chao Dong, Yu Qiao, and Chen Change Loy. Esrgan: Enhanced super-resolution generative adversarial networks. In *Proceedings of the European conference on computer vision (ECCV) workshops*, pages 0–0, 2018.
- [56] Yuxin Wang, Chu-Tak Lee, Qipeng Guo, Zhangyue Yin, Yunhua Zhou, Xuanjing Huang, and Xipeng Qiu. What dense graph do you need for self-attention? In *International Conference on Machine Learning*, pages 22752–22768. PMLR, 2022.
- [57] Shaoan Xie, Zhifei Zhang, Zhe Lin, Tobias Hinz, and Kun Zhang. Smartbrush: Text and shape guided object inpainting with diffusion model. *arXiv preprint arXiv:2212.05034*, 2022.
- [58] Wenhan Xiong, Barlas Oğuz, Anchit Gupta, Xilun Chen, Diana Liskovich, Omer Levy, Wen-tau Yih, and Yashar Mehdad. Simple local attentions remain competitive for long-context tasks. *arXiv preprint arXiv:2112.07210*, 2021.
- [59] Zongxin Yang, Jian Dong, Ping Liu, Yi Yang, and Shuicheng Yan. Very long natural scenery image prediction by outpainting. In *Proceedings of the IEEE/CVF International Conference on Computer Vision*, pages 10561–10570, 2019.
- [60] Jinyang Yuan, Tonglin Chen, Bin Li, and Xiangyang Xue. Compositional scene representation learning via reconstruction: A survey. *IEEE Transactions on Pattern Analysis and Machine Intelligence*, 2023.
- [61] Manzil Zaheer, Guru Guruganesh, Kumar Avinava Dubey, Joshua Ainslie, Chris Alberti, Santiago Ontanon, Philip Pham, Anirudh Ravula, Qifan Wang, Li Yang, et al. Big bird: Transformers for longer sequences. *Advances in neural information processing systems*, 33:17283–17297, 2020.

6 Supplementary Materials

In the Supplementary Materials, we first provide the proofs of the main conclusions in Section 3, then we introduce the involved existing assets, evaluation settings and computing infrastructure, and finally we show the additional experimental results on our method for the performance comparison.

6.1 Proofs

In this section, we provide the proofs of the connection between attention entropy and token number, which constitutes the main conclusion in Section 3.

Let $\mathbf{X} \in \mathbb{R}^{N \times d}$ denotes an image token sequence to an attention module, where N, d are the number of tokens and the token dimension, respectively. We then denote the key, query and value matrices as $\mathbf{K} = \mathbf{X}\mathbf{W}^K$, \mathbf{Q} and \mathbf{V} , where $\mathbf{W}^K \in \mathbb{R}^{d \times d_r}$ is a learnable projection matrix. The attention layer ([3; 52]) computes $\text{Attention}(\mathbf{Q}, \mathbf{K}, \mathbf{V}) = \mathbf{A}\mathbf{V}$ with the attention map \mathbf{A} calculated by the row-wise softmax function as follows:

$$\mathbf{A}_{i,j} = \frac{e^{\lambda \mathbf{Q}_i \mathbf{K}_j^\top}}{\sum_{j'=1}^N e^{\lambda \mathbf{Q}_i \mathbf{K}_{j'}^\top}}, \quad (8)$$

where λ is a scaling factor, usually set as $1/\sqrt{d}$ in the widely-used Scaled Dot-Product Attention [52] and i, j are the row indices on the matrices \mathbf{Q} and \mathbf{K} , respectively. Following [2; 12], we calculate the attention entropy by treating the attention distribution of each token as a probability mass function of a discrete random variable. The attention entropy with respect to i^{th} row of \mathbf{A} is defined as:

$$\text{Ent}(\mathbf{A}_i) = - \sum_{j=1}^N \mathbf{A}_{i,j} \log(\mathbf{A}_{i,j}), \quad (9)$$

We now investigate the relation between the attention entropy and the token number. By substituting Eq.(1) into Eq.(2), we have:

$$\begin{aligned} \text{Ent}(\mathbf{A}_i) &= - \sum_{j=1}^N \left[\frac{e^{\lambda \mathbf{Q}_i \mathbf{K}_j^\top}}{\sum_{j'=1}^N e^{\lambda \mathbf{Q}_i \mathbf{K}_{j'}^\top}} \log \left(\frac{e^{\lambda \mathbf{Q}_i \mathbf{K}_j^\top}}{\sum_{j'=1}^N e^{\lambda \mathbf{Q}_i \mathbf{K}_{j'}^\top}} \right) \right] \\ &= \log \sum_{j=1}^N e^{\lambda \mathbf{Q}_i \mathbf{K}_j^\top} - \frac{\sum_{j=1}^N (e^{\lambda \mathbf{Q}_i \mathbf{K}_j^\top} \lambda \mathbf{Q}_i \mathbf{K}_j^\top)}{\sum_{j=1}^N e^{\lambda \mathbf{Q}_i \mathbf{K}_j^\top}} \\ &= \log N + \log \left(\frac{1}{N} \sum_{j=1}^N e^{\lambda \mathbf{Q}_i \mathbf{K}_j^\top} \right) - \frac{\frac{1}{N} \sum_{j=1}^N (e^{\lambda \mathbf{Q}_i \mathbf{K}_j^\top} \lambda \mathbf{Q}_i \mathbf{K}_j^\top)}{\frac{1}{N} \sum_{j=1}^N e^{\lambda \mathbf{Q}_i \mathbf{K}_j^\top}} \\ &\approx \log N + \log \mathbb{E}_j(e^{\lambda \mathbf{Q}_i \mathbf{K}_j^\top}) - \frac{\mathbb{E}_j(\lambda \mathbf{Q}_i \mathbf{K}_j^\top e^{\lambda \mathbf{Q}_i \mathbf{K}_j^\top})}{\mathbb{E}_j(e^{\lambda \mathbf{Q}_i \mathbf{K}_j^\top})}, \end{aligned} \quad (10)$$

where \mathbb{E}_j denotes the expectation upon the index j , and the last equality holds asymptotically when N gets larger.

Given \mathbf{X} as an encoded sequence from an image, we assume each token \mathbf{X}_j as a vector sampled from a multivariate Gaussian distribution $\mathcal{N}(\boldsymbol{\mu}^X, \boldsymbol{\Sigma}^X)$. This widespread assumption is shared by multiple works [14; 20; 28] in image synthesis and style transfer. In this way, each $\mathbf{K}_j = \mathbf{X}_j \mathbf{W}^K$ could be considered as a sample from a multivariate Gaussian distribution $\mathcal{N}(\boldsymbol{\mu}^K, \boldsymbol{\Sigma}^K) = \mathcal{N}(\boldsymbol{\mu}^X \mathbf{W}^K, (\mathbf{W}^K)^\top \boldsymbol{\Sigma}^X \mathbf{W}^K)$. In regard to \mathbf{K}_j , its dimension-wise linear combination $y_i = \lambda \mathbf{Q}_i \mathbf{K}_j^\top$ could be treated as a scalar random variable sampled from a Gaussian distribution $y_i \sim \mathcal{N}(\mu_i, \sigma_i^2) = \mathcal{N}(\lambda \mathbf{Q}_i (\boldsymbol{\mu}^K)^\top, \lambda^2 \mathbf{Q}_i \boldsymbol{\Sigma}^K \mathbf{Q}_i^\top)$. Under this circumstance, we dive into the expectations $\mathbb{E}_j(e^{\lambda \mathbf{Q}_i \mathbf{K}_j^\top})$

and $\mathbb{E}_j(\lambda \mathbf{Q}_i \mathbf{K}_j^\top e^{\lambda \mathbf{Q}_i \mathbf{K}_j^\top})$ in Eq.(3):

$$\begin{aligned}
\mathbb{E}_j(e^{\lambda \mathbf{Q}_i \mathbf{K}_j^\top}) &\doteq \mathbb{E}_j(e^{y_i}) \\
&= \int e^{y_i} \frac{1}{\sqrt{2\pi}\sigma_i} e^{-\frac{y_i^2 - 2\mu_i y_i + \mu_i^2}{2\sigma_i^2}} dy_i \\
&= \int \frac{1}{\sqrt{2\pi}\sigma_i} e^{-\frac{(y_i - \mu_i - \sigma_i^2)^2}{2\sigma_i^2}} e^{\mu_i + \frac{\sigma_i^2}{2}} dy_i \\
&= e^{\mu_i + \frac{\sigma_i^2}{2}} \\
\mathbb{E}_j(\lambda \mathbf{Q}_i \mathbf{K}_j^\top e^{\lambda \mathbf{Q}_i \mathbf{K}_j^\top}) &\doteq \mathbb{E}_j(y_i e^{y_i}) \\
&= \int y_i e^{y_i} \frac{1}{\sqrt{2\pi}\sigma_i} e^{-\frac{y_i^2 - 2\mu_i y_i + \mu_i^2}{2\sigma_i^2}} dy_i \\
&= \int y_i \frac{1}{\sqrt{2\pi}\sigma_i} e^{-\frac{(y_i - \mu_i - \sigma_i^2)^2}{2\sigma_i^2}} e^{\mu_i + \frac{\sigma_i^2}{2}} dy_i \\
&= (\mu_i + \sigma_i^2) e^{\mu_i + \frac{\sigma_i^2}{2}},
\end{aligned} \tag{11}$$

By substituting Eq.(4) into Eq.(3), we have:

$$\begin{aligned}
\text{Ent}(\mathbf{A}_i) &= \log N + \log(e^{\mu_i + \frac{\sigma_i^2}{2}}) - \frac{(\mu_i + \sigma_i^2) e^{\mu_i + \frac{\sigma_i^2}{2}}}{e^{\mu_i + \frac{\sigma_i^2}{2}}} \\
&= \log N + \mu_i + \frac{\sigma_i^2}{2} - (\mu_i + \sigma_i^2) \\
&= \log N - \frac{\sigma_i^2}{2}.
\end{aligned} \tag{12}$$

In this way, we reach the connection between attention entropy and token number, which lays a solid theoretical foundation for the subsequent interpretations and the scaling factor proposed.

6.2 Implementation details

In this section, we provide the detailed implementation settings in Section 4, including involved existing assets, evaluation settings, computing infrastructure, etc.

6.2.1 Involved existing assets.

For the evaluation code, we refer to the github code repository called Diffusers (URL) released by Hugging face with Apache License, Version 2.0. The revised code are shown in Algorithm 1.

For the model parameters, we select the stable diffusion parameters released by stability AI ([38], version: stable-diffusion-2-1-base, URL) and the latent diffusion parameters released by CompVis ([38], version: ldm-text2im-large-256, URL). Both of them are top-ranked parameter files for downloading.

For datasets, we use LAION-400M ([44], URL) and LAION-5B dataset ([43], URL), which contain over 400 million and 5.85 billion CLIP-filtered image-text pairs, respectively.

6.2.2 Evaluation settings

We evaluate two scaling factors on a subset of LAION-400M and LAION-5B dataset. We randomly select 30K image-text data pairs from LAION-5B and 50K image-text data pairs from LAION-400M, respectively. We then synthesize corresponding 30K images upon LAION-5B text data with stable diffusion model and 50K images upon LAION-400M text data with latent diffusion model. We compute corresponding FID-30K (Stable diffusion) and FID-50k (Latent diffusion) with synthesized images and original images from datasets.

Algorithm 1 Replace the scaling factor

Require: Token number during training $T \geq 0$, Flag to replace the scaling factor C

Ensure: $\lambda = \sqrt{\log_T N/d}$

$\mathbf{Q} \leftarrow \mathbf{XW}_Q$

$\mathbf{K} \leftarrow \mathbf{XW}_K$

$\mathbf{V} \leftarrow \mathbf{XW}_V$

if C is True **then**

$\lambda \leftarrow \sqrt{\log_T N/d}$

else if C is False **then**

$\lambda \leftarrow \sqrt{1/d}$

end if

$\text{Attn} = \text{softmax}(\lambda \mathbf{QK}^\top) \mathbf{V}$

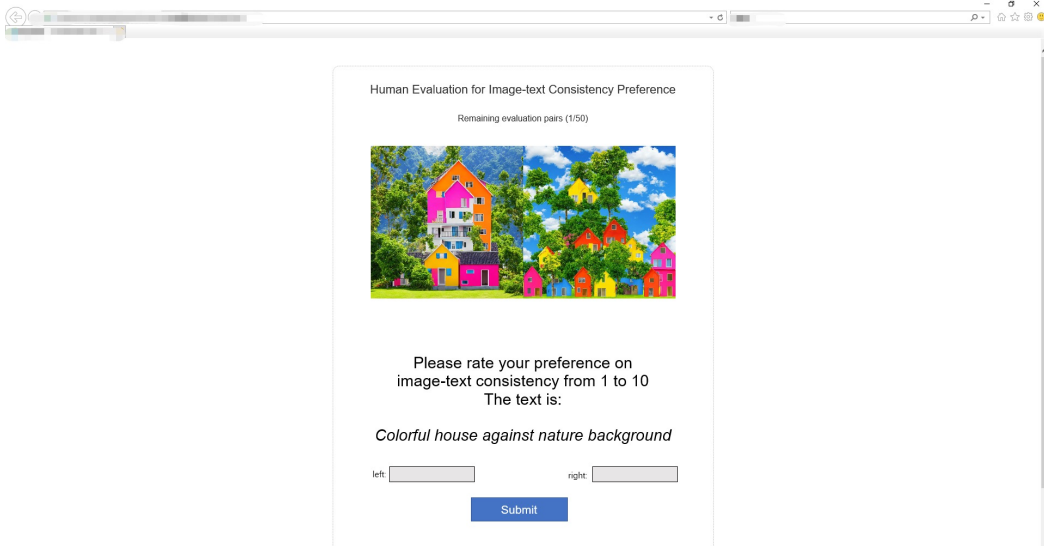


Figure 8: The screenshot of our human evaluation website.

6.2.3 Computing infrastructure

Experiments are conducted on a server with Intel(R) Xeon(R) Gold 6226R CPUs @ 2.90GHz and four NVIDIA Tesla A100 GPUs. The code is developed based on the PyTorch framework with version 1.9.1.

6.2.4 Human evaluation details

We conduct an text-based pairwise preference test. For a specific context, we pair the synthesized image of our method with the synthesized image from the baseline and ask 45 annotators to give each response a rating score for consistency. We randomly select 50 pairs of images-text data (two images from two methods and a corresponding text prompt) and show them to 45 participants to rate from 1 to 10. We observe that users rate higher for our method, which suggests that the synthesized images from our method are more contextually coherent with texts than the baseline. Besides, with the refinement from the proposed scaling factor, the generated contents from our model are able to convey more natural and informative objects. The screenshot is depicted in Figure 8.

6.3 Broader impacts

Our approach focuses on synthesizing images with a high level of fidelity, which raises concerns about potential impacts in a broader context, specifically related to the misuse of portraits. Notably, when our method is provided with prompts referencing highly popular celebrities, it consistently

Table 4: FID, memory usage and time cost of stable diffusion with multiple settings for different resolutions. The results for low resolution demonstrate that our method could achieve better performance in memory usage and time cost with trade-off in fidelity.

Resolutions	FID (\downarrow)	GPU Memory (MiB) (\downarrow)	Average Time (s) (\downarrow)
128 * 128 (Original)	191.5447	6867	3.4953
128 * 128 (Ours)	127.2798	6867	3.4955
512 * 512 and Resize to 128	36.0742	9324	17.4377
224 * 224 (Original)	74.5742	7064	5.6268
224 * 224 (Ours)	41.8925	7064	5.6274
512 * 512 and Resize to 224	21.8415	9324	17.4457

Table 5: FID (4K samples), memory usage and time cost of our method and MultiDiffusion[4]. Our method outperforms MultiDiffusion on each metric except for the GPU Memory.

Resolutions	FID (\downarrow)	GPU Memory (MiB) (\downarrow)	Average Time (s) (\downarrow)
224 * 224 (Ours)	50.3515	7064	5.6274
224 * 224 (MD)	154.6925	7061	31.7680
768 * 768 (Ours)	28.1372	19797	36.7140
768 * 768 (MD)	40.9270	9906	122.2485

generates figures that bear a strong resemblance to the mentioned individuals. Consequently, there is a risk of portrait misusing or even the infringement of portrait rights.

It is worth acknowledging that the potential impact mentioned above is not unique to our method but is a challenge faced by most image synthesis techniques. We firmly believe that numerous researchers have already recognized and been working on this issue with utmost seriousness and diligence.

6.4 Additional experimental results

In this section, we provide more qualitative and quantitative results for the validation of our theoretical findings and the proposed scaling factor.

6.4.1 Quantitative results

In Table 1, we present FID, memory usage and time cost of stable diffusion with multiple settings for the text-to-image synthesis of various resolutions (128^2 , 224^2 , 768^2 , 1024^2). For low resolution, our method achieves better performance in memory usage and time cost with trade-off in fidelity. Considering the high demand for memory and time resources (especially for portable devices), we believe the trade-off is acceptable.

In Table 2, We compare our method with MultiDiffusion[4] and report corresponding FID(4K samples), memory usage and time cost. As it is shown, our method outperforms MultiDiffusion on each metric except for the GPU Memory.

6.4.2 Qualitative results

As shown in Figure 9, 10 and 11, our scaling factor manages to synthesize objects with better visual effect in lower resolution images, outperforming the original scaling which depicts visual concepts in a rough manner. From Figure 12 and 13, our scaling factor does better in naturally organizing visual concepts portrayal in higher resolution images, surpassing the original scaling factor in image presentations.



Figure 9: **Qualitative comparison** on the scale factors for the resolution 224×224 . The original scaling factor misses out content or roughly depicts the objects in prompts while our scaling factor manages to synthesize visual concepts in high fidelity and better illumination. Please zoom in for better visual effect.

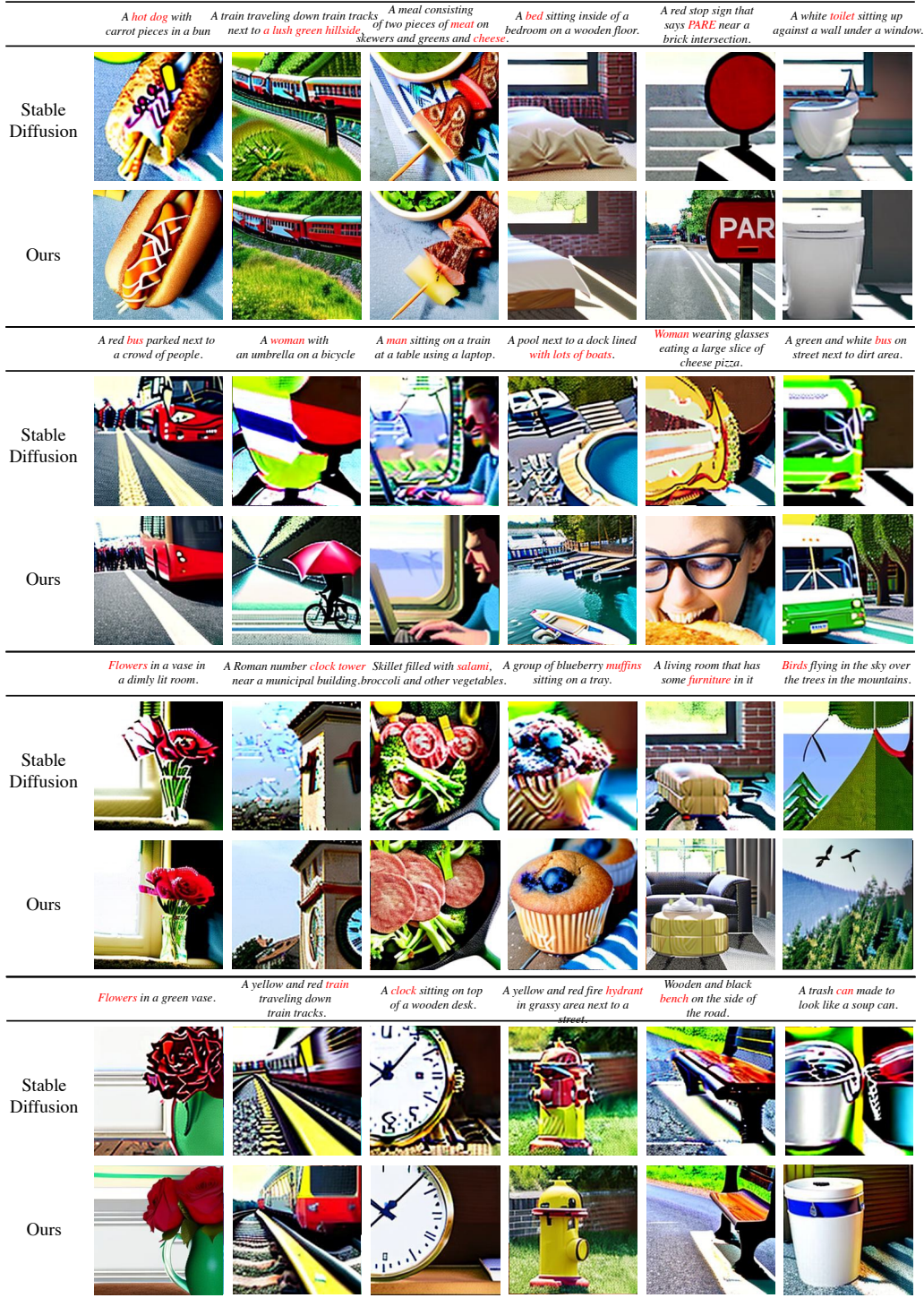


Figure 10: **Qualitative comparison** on the scale factors for the resolution 224×224 . The original scaling factor misses out content or roughly depicts the objects in prompts while our scaling factor manages to synthesize visual concepts in high fidelity and better illumination. Please zoom in for better visual effect.






















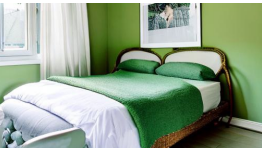


	<i>A skateboarder catches major air during this stunt.</i>	<i>A small white bird standing on top of a dirt field.</i>	<i>A bathroom with a sink, toilet, tub and mirror.</i>
Stable Diffusion			
Ours			
	<i>A man giving a little boy a hair cut.</i>	<i>A kite that is laying down in the sand.</i>	<i>Two men on surfboards riding on a small wave.</i>
Stable Diffusion			
Ours			
	<i>A kitchen in a restaurant with several hot dogs on a grill with some buns.</i>	<i>A dish of pancakes covered in bananas A weather vane with a clock near a body of water.</i>	
Stable Diffusion			
Ours			
	<i>A green netted bed in a light filled bedroom.</i>	<i>A woman looks around a very small kitchen.</i>	<i>A man standing next to an elephant with a long trunk.</i>
Stable Diffusion			
Ours			

Figure 11: **Qualitative comparison** on the scale factors for the resolution 512×288 . The original scaling factor misses out content or roughly depicts the objects in prompts while our scaling factor manages to synthesize visual concepts in high fidelity and better illumination. Please zoom in for better visual effect.

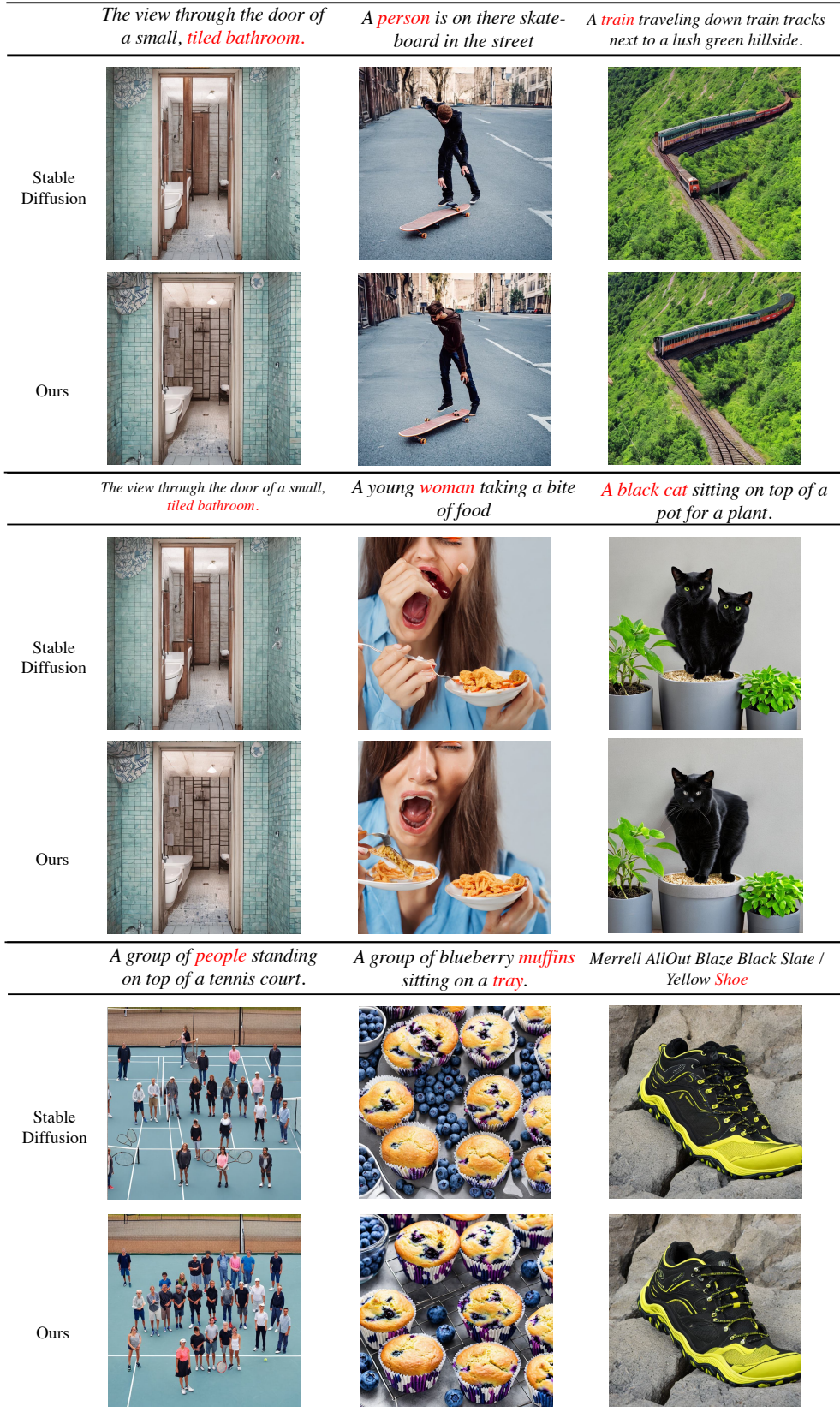


Figure 12: **Qualitative comparison** on the scale factors for the resolution 768×768 . The original scaling factor depicts the objects in a repetitive and unorganized pattern while our scaling factor manages to synthesize visual concepts in high fidelity. Please zoom in for better visual effect.

Stable
Diffusion



Prompt: Colorful house against nature background.

Ours



Figure 13: **Qualitative comparison** on the scale factors for the resolution 1024×1024 .